PL ISSN 0033-2097, e-ISSN 2449-9544

10'2024

PRZEGLĄD ELEKTROTECHNICZNY

ROK 100

WYDAWNICTWO SIGMA-NOT

cena 85 zł
(w tym 8% VAT)

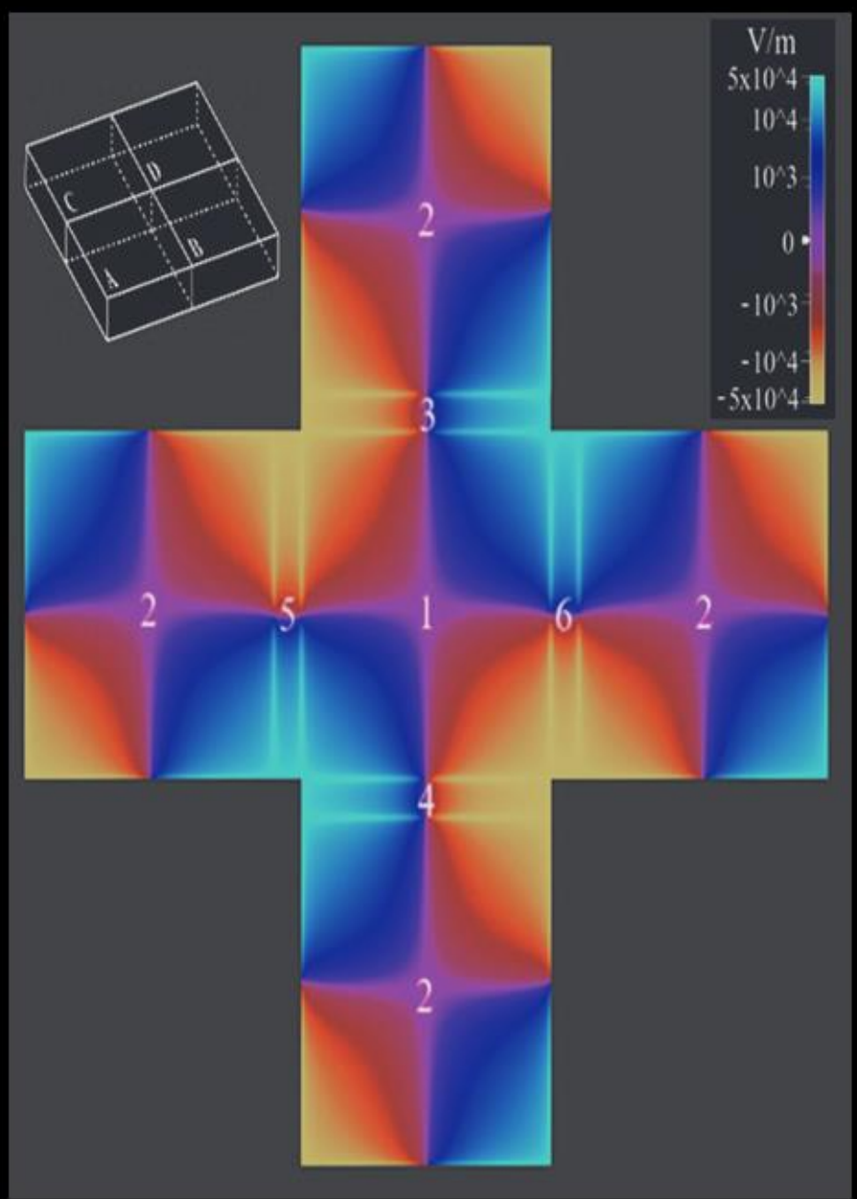

Relaksacja elektryzacji metalowego obiektu po zakłóceniu intencjonalnym impulsowym zaburzeniem elektromagnetycznym
Str 269

PRZEGLĄD ELEKTROTECHNICZNY Vol 2024, Nr 10

Spis treści

01 **Marcin SMOŁKA, Roman KORAB, Marcin POŁOMSKI[3] -** Minimalizacja wpływu prosumenckich mikroinstalacji fotowoltaicznych na pracę sieci niskiego napięcia 1

02 **Bogdan FABIANSKI , Tomasz PAJCHROWSKI, Krzysztof ZAWIRSKI -** Przetwarzanie sygnału momentomierza Futek TRS705 oraz komunikacja wewn ˛etrza w zautomatyzowanym stanowisku badawczym nap ˛edu z silnikiem reluktancyjnym przeł ˛aczalnym 7

03 **Andrzej GĘBURA, Andrzej SZELMANOWSKI, Marek BRZOZOWSKI -** Możliwości zastosowania systemów fotowoltaicznych w technologiach wojskowych 16

04 **Dariusz WIĘCEK, Marcin MORA -** Warunki kompatybilności systemów IMT 4G/5G z telewizją naziemną DVB-T/T2 w paśmie 700 MHz 27

05 **Krzysztof HABELOK, Kamil GRUSZCZYK , Paweł LASEK, Mariusz STĘPIEŃ -** Wyznaczanie zależności kątowej prądu krytycznego I_c w wysokotemperaturowych taśmach nadprzewodnikowych 1G 35

06 **Saadat Shikhaliyeva, Elshad Safiyev -** Rozwiązywanie problemów optymalizacyjnych w pracy ustalonej regulowanego silnika asynchronicznego 39

07 **Aldi SAPUTRA, Rendra GUSTRIANSYAH, Ahmad SANMORINO[*], Zaid Romegar MAIR, Dewi SARTIKA, Shinta PUSPASARI -** Prognozowanie liczby pasażerów w transporcie szynowym przy użyciu sezonowej autoregresyjnej zintegrowanej średniej ruchomej (SARIMA 43

08 **Hryhorii KALETNIK, Vitalii YAROPUD,** Badanie procesu nagrzewania przepływu powietrza w pionowym gruntowym wymienniku ciepła 46

09 **Imene SOUICI, Izzeddine CHALABI, Lahouaoui Lalaoui -** Modelowanie bałaganu morskiego przy użyciu złożonego rozkładu Gaussa z teksturą Nakagami i szumem termicznym 55

10 **Ulkar Ashurova -** Reżimy temperaturowe przewodów parownika przy częściowym obciążeniu bloków energetycznych 59

11 **Wipobh JAIKHANG, Puchong CHANJIRA -** Optymalizacja regulatora PI przy użyciu algorytmu kolonii mrówek dla systemu turbin wiatrowych 64

12 **Pawan Kumar PANDEY, Ramesh KUMAR, Manish SINGLA, Sergey KOKIN, Murodbek SAFARALIEV, Javod AHYOEV –** Automatyczna korekcja współczynnika mocy za pomocą mikrokontrolera w sektorze energetycznym 69

13 **Santoso, Ratna Hartayu, Ahmad Ridho'i, Aris Heri Andriawan, Wahyu Setyo Pambudi, Ahmad Nuril Anwar, Syahri Muharom `-** Analiza uszkodzeń łożysk wykorzystująca metodologię logiki rozmytej w celu zwiększenia dokładności diagnostyki 73

14 **Zoran MILIVOJEVIĆ, Ratko IVKOVIĆ, Bojan PRLINČEVIĆ, Dijana KOSTIĆ -** Optymalizacja jądra wielomianowej interpolacji piątego rzędu 1P w dziedzinie czasu 79

15 **Persiya Gnana Golda. D, D.S. Shylu Sam, P.Sam Paul, D.Jayanthi -** Przetwornik ADC Flash o niskim poborze mocy 100 MS/s z techniką kodowania kodu termometru do zastosowań motoryzacyjnych 84

16 **Abdelghafour HERIZI, Abderrahim ZEMMIT, Riyadh ROUABHI, Fayssal OUAGUENI -** Nowa konstrukcja solidnego sterownika opartego na 12 rozmytych zmiennych lingwistycznych dla systemu konwersji energii wiatru 89

17 **Jerushan J, Kevin Enoch, Vincent Sam Jebadurai S[*], Hemalatha G, Arunraj E, Ringle Raja S, Nirmala T, Brindha D - Integracja danych skanowania w celu ulepszenia BIM: przegląd technik, strategii mapowania i aplikacji cyklu życia budynku** 93

18 **Nuhu Stephen Tagwai, Nik Noordini Nik Abd Malik, Mohammad Rijal Hamid -** A Analiza porównawcza wpływu powierzchni selektywnych częstotliwościowo o kształcie koła, kwadratu i sześciokąta na wydajność anteny mikropaskowej 10 GHz 101

19 **Betim MALOKU, Pelqim SPAHIU -** Maksymalizacja efektywno ´sci energetycznej sieci mobilnych pi ˛atej generacji (5G) w poci ˛agach du ˙zych pr ˛edko ´sci 107

20 **El Mouatez Billah Messini, Yacine Bourek, Chouaib Ammari -** Szacowanie techniczno-ekonomiczne produkcji wodoru z jednego modułu fotowoltaicznego w regionie Hassi Messaoud – Algieria 113

21 **Fethi CHOUAF, Yacine DJEGHADER, Choayb BOUSNOUBRA -** Poprawa jakości zasilania przy użyciu hybrydowych filtrów zasilania z nieliniowym sterownikiem 118

22 **Muldi YUHENDRI, Risfendra, Emilham MIRSHAD, Adam R. SIDIQI[1]-** Sterowanie w czasie rzeczywistym silnikiem prądu stałego o oddzielnym wzbudzeniu w oparciu o układ Fuzzy PI z wykorzystaniem Arduino 123

23 **Fatima Zohra RAHOU -** Numeryczna symulacja pojedynczej studni kwantowej diody UV LED na bazie AlGaN/GaN/AlGaN 128

24 **Sergei PETRICHENKO, Krzysztof PRZYSTUPA, Antonina MALYUSHEVSKAYA, Artem IVANOV, Olena MITRYASOVA, Orest KOCHAN -** Wpływ indukcyjności obwodu wyładowczego na proces oczyszczania odpadów galwanicznych metodą elektroiskrową 132

25 **Dmytro MAMCHUR, Oleksandr KASICH, Andrii KALINOV** - Diagnostyka silnika indukcyjnego oparta na analizie sygnałów elektrycznych przy wykorzystaniu technologii chmurowyc 136

26 **Dorota JACKIEWICZ -** Wykorzystanie przybliżenia Rayleigha do analizy efektu magnetosprężystego w elementach kratownicy 140

27 **Dominika KOPALA, Roman SZEWCZYK, Anna OSTASZEWSKA-LIŻEWSKA -** Poprawiona dokładność modeli FEM fluxgate opartych na adaptacyjnym siatkowaniu 143

28 **Adam GARCZAREK, Dorota STACHOWIAK -** Układ cewek Helmholtza do testowania mierników pola stosowanych do pomiaru pól magnetycznych generowanych przez pojazdy trakcyjne 147

29 **David UKWUNGWU, Nora LEUNING, Kay HAMEYER[1]-** Symulacja wpływu pakowania zgrzewanego na właściwości elektromagnetyczne blach elektrotechnicznych przy użyciu lokalnego modelu materiału zmiennego 152

30 **Jacek SALACH -** Wpływ przetwarzania sygnału na czułość czujnika momentu magneto-sprężystego 156

31 **Paweł JABŁOŃSKI, Krzysztof CHWASTEK, Mariusz NAJGEBAUER, Dariusz KUSIAK, Tomasz SZCZEGIELNIAK, Branko KOPRIVICA, Marko ROSIĆ, Srdjan DIVAC -** Modelowanie wpływu częstotliwości wzbudzenia na kształt pętli histerezy w permaloju 160

PRZEGLĄD ELEKTROTECHNICZNY Vol 2024, Nr 10

Spis treści

32	**Tomasz GARSTKA, Marcin KWAPISZ, Marlena KRAKOWIAK, Sylwester SAWICKI -** Głowica pomiarowa robota dla zautomatyzowanych pomiarów szumu Barkhausena	164
33	**Marek HRECZKA, Wojciech BURLIKOWSKI, Marta DUDEK-BURLIKOWSKA, Janusz HETMAŃCZYK, Aleksandra Kolano-BURIAN, Roman KOLANO[1]-** Analiza wpływu parametrów nowego materiału magnetycznego o niskiej stratności rdzenia stojana na sprawność silnika elektrycznego szybkoobrotowego	168
34	**Wojciech A. PLUTA -** Modelowanie kierunkowej straty mocy blach elektrotechnicznych przy namagnesowaniu osiowym	173
35	**Wiesław CITKO, Damian HALLMANN, Łukasz WOJEWÓDKA** - Badania parametrów statystycznych sygnałów hydroakustycznych	177
36	**Adam KONIECZKA, Hubert ANTCZAK, Patryk KACZMAREK, Dawid SZWARC -** Zastosowanie biblioteki SFML do modelowania ruchu ulicznego na skrzyżowaniu z sygnalizacją świetlną	181
37	**Robert PICH, Agnieszka GONCIARZ, Marek BŁĘDOWSKI, Rafał KOTAPKA -** Dekontaminacja nośników danych stanowiących podłoża śladów kryminalistycznych	185
38	**Maciej KAWKA -** Wieloetapowy algorytm naprowadzania na cel obiektu BSP	189
39	**Krzysztof POSOBKIEWICZ**, **Krzysztof GÓRECKI -** Wpływ rozrzutu technologicznego parametrów tranzystorów MOS mocy na dokładność pomiaru ich rezystancji termicznej	195
40	**Adam KONIECZKA, Karolina BROŃCZYK, Michał ADAMSKI, Agata DĄBROWSKA, Adam DĄBROWSKI -** Urządzenie do szybkiego oznaczania formaldehydu uwalnianego z naczyń ekologicznych do żywności	199
41	**Jakub KONOPIŃSKI, Krystyna BARAN, Jakub ŁAZIK, Piotr GÓRAL, Paweł PAWŁOWSKI -** Sztuczna sieć neuronowa kontra technika algorytmiczna w zadaniu klasyfikacji kształtów	204
42	**Julian BALCEREK, Adam DĄBROWSKI, Paweł PAWŁOWSKI -** Sygnały i systemy wizyjne w modelu automatyzacji pojazdów	208
43	**Julian BALCEREK, Adam DĄBROWSKI, Paweł PAWŁOWSKI, Piotr TOKARSKI -** Automatyczne rozpoznawanie elementów polskich pojazdów historycznych	212
44	**Zenon KIDOŃ -** Rozdzielczość pomiaru współrzędnych punktu trajektorii w teście stabilografii nadążnej	216
45	**Sebastian SZYMAŃSKI, Krzysztof GÓRSKI, Korneliusz SIERPOWSKI, Igor MIELCZAREK, Jakub GRZESIAK, Maciej KOWAL -** Koncepcja systemu kontroli, sterowania i zarządzania BSP wykorzystującego technologię wirtualnej i rozszerzonej rzeczywistości	220
46	**Jakub GRZESIAK, Krzysztof GÓRSKI, Sebastian SZYMAŃSKI, Korneliusz SIERPOWSKI, Igor MIELCZAREK, Alan KASPERCZAK** - Zastosowanie algorytmów rozpoznawania obrazu w Bezzałogowych Statkach Powietrznych	224
47	**Korneliusz SIERPOWSKI, Grzegorz DEBITA, Jakub GRZESIAK, Igor MIELCZAREK, Sebastian SZYMAŃSKI, Monika ZAMŁYŃSKA, Krzysztof GÓRSKI -** Pokładowy system identyfikacji kamuflażu “swój- obcy” dedykowany BSP rozpoznawczym	228
48	**Adam MUC[1], Andrzej KASPROWICZ, Agata BIELECKA, Piotr MYSIAK, Jan IWASZKIEWICZ -** Wpływ potencjału odniesienia na pracę układu formowania impulsów 12-pulsowego prostownika sterowanego	232
49	**Przemysław PTAK, Krzysztof GÓRECKI, Paweł GÓRECKI, Emilian ŚWITALSKI -** Niezależna od sieci elektroenergetycznej mobilna stacja ładowania pojazdów elektrycznych	236
50	**Kalina DETKA, Michał DOWNAR-ZAPOLSKI, Krzysztof GÓRECKI -** Porównanie wybranych narzędzi do symulacji przetwornic dc-dc	241
51	**Krzysztof GÓRECKI, Ewa KRAC -** Wpływ sposobu połączenia fotoogniw w panelu fotowoltaicznym na jego odporność na częściowe zacienienie	246
52	**Jan MOCHA, Grzegorz BADURA, Grzegorz NOWAK, Aleksander SOBOTNICKI, Paweł KOSTKA -** Modułowa architektura urządzenia do elektroporacji ze sprzętowo-programowym układem bezpieczeństwa	250
53	**Adam MUC[1]-** Współpraca różnych - co do liczby poziomów i trójfazowych falowników napięcia z wykorzystaniem teorii przestrzennych wektorów ortogonalnych	254
54	**Kalina DETKA, Tomasz OLZAK, Krzysztof GÓRECKI -** Analiza właściwości przetwornicy SEPIC z dławikiem sprzężonym	258
55	**Magdalena BUDNAROWSKA, Jerzy MIZERACZYK -** Prototyp metamateriałowego systemu harwestera mikrofalowego	261
56	**Magdalena BUDNAROWSKA , Jerzy MIZERACZYK -** Skuteczność ekranowania wnętrza małej obudowy z otworem przed subnanosekundowym impulsem EM o polaryzacji równoległej	265
57	**Jerzy MIZERACZYK , Magdalena BUDNAROWSKA, Filip FALKOWSKI -** Relaksacja elektryzacji metalowego obiektu po zakłóceniu intencjonalnym impulsowym zaburzeniem elektromagnetycznym	269
58	**Dawid BUDNAROWSKI, Łukasz DŁUGOŃSKI, Kalina DETKA, Magdalena SKOTNICKA -** Zastosowanie rozszerzonej rzeczywistości w edukacji żywieniowej dzieci	273
59	**Sergii BESPALKO, Marcin SIEDLECKI, Justyna MARKIEWICZ, Jerzy MIZERACZYK -** Wpływ pośredniej sonikacji na powstawanie plazmy i charakterystykę energetyczną w reżimie katodowym plazmowej elektrolizy roztworu	277
60	**Adam MUC**, **Jan IWASZKIEWICZ -** Pięciofazowy falownik kaskadowy sterowany wektorami obliczonymi na podstawie falki Haara)	281
61	**Emilian ŚWITALSKI, Krzysztof GÓRECKI -** Otwarte i warstwowe projektowanie sterowników PLC na przykładzie sterownika do zastosowań edukacyjnych	285
62	**Joanna PATRZYK, Janusz ZARĘBSKI, Damian BISEWSKI -** Charakterystyki i parametry tranzystora SiC BJT	289
63	**Idris KUSUMA, R. RULIYANTA, Diah WIDIASTUTI, Mohammad FATHONI -** Optymalizacja oszczędności energii elektrycznej poprzez wykorzystanie katalizatorów chłodniczych w sprężarkach	294

1. Hryhorii KALETNIK[1], 2. Vitalii YAROPUD[1], 3. Svitlana LUTKOVSKA[1], 4. Elchyn ALIIEV[2]

Vinnytsia National Agrarian University (1), Dnipro State Agrarian and Economic University (2)
ORCID. 1. 0000-0002-4848-2796, 2. 0000-0003-0502-1356,
3. 0000-0002-8350-5519; 4. 0000-0003-4006-8803

doi:10.15199/48.2024.10.08

Studying the air flow heating process in the vertical type ground heat exchanger

***Abstract**. The article presents the results of analytical studies of air losses of vertical ground heat exchangers for two proposed schemes (concentric and U-shaped). The distribution of the temperature field during the summer and winter periods was obtained through numerical simulation of the air heating process in concentric and U-shaped vertical ground heat exchangers using the Simcenter Star-CCM+ software package.*

Streszczenie.** W artykule przedstawiono wyniki badań analitycznych strat powietrza w pionowych gruntowych wymiennikach ciepła dla dwóch zaproponowanych schematów (koncentrycznego i U-kształtnego). Rozkład pola temperatur w okresie letnim i zimowym uzyskano poprzez symulację numeryczną procesu nagrzewania powietrza w koncentrycznych i pionowych gruntowych wymiennikach ciepła w kształcie litery U z wykorzystaniem pakietu oprogramowania Simcenter Star-CCM+.* (Badanie procesu nagrzewania przepływu powietrza w pionowym gruntowym wymienniku ciepła***)

Keywords: soil heat exchanger, numerical modeling, experimental studies, pneumatic losses, effective heat capacity.
Słowa kluczowe: gruntowy wymiennik ciepła, modelowanie numeryczne, badania eksperymentalne, straty pneumatyczne.

Introduction

Global trends of growing prices for traditional fuel resources used for electricity generation require agricultural enterprises to diversify electricity supply sources and increase the level of power autonomy. Despite the widespread present-day opinion regarding the low efficiency of wind and solar energy utilization in Ukraine's natural and climatic conditions, the experience of highly developed countries testifies to the contrary:

- implementation of projects related to introduction of autonomous power supply systems for agro-industrial enterprises based on SPPs and WPPs has environmental and economic advantages over traditional power supply [1];
- today's development of technologies makes it possible to convert of solar and wind energy into electric power in the territories that were previously (20-30 years ago) considered unsuitable for this type of energy [2].

Development of the organic sector is particularly significant and promising for domestic farmers, consumers and the state as a whole, especially in the context of ensuring food supply security, healthy nutrition and preservation of natural environment. In accordance with strategic goal 1 "Ensuring a stimulating and reasonable agro-policy" being part of the Strategic policy course in the field of agro-industrial sector development, one of the ways to achieve the strategic goal lies in support of organic production. Another way to achieve the goal is to ensure the development of sustainable production, in which respect the Government's task is defined as encouragement of sustainable agricultural production, protection of environment and fauna, spreading the use of organic production methods and the use of biotechnology, "climate-smart" agriculture and forestry along with reduction of greenhouse gas emissions and adaptation to climate change, sustainable management of natural resources, as well as biodiversity preservation and augmentation [3].

The livestock breeding sector of agro-industrial production has the greatest potential for increase of power use efficiency. It can be seen that the power used for air cooling makes a significant part of total energy consumption, which is constantly increasing due to increased requirements for maintenance of optimal microclimate in livestock premises [4, 5].

The largest share of power consumption in livestock breeding premises falls on generation of standard microclimate parameters, particularly those required for heating of supplied ventilation air. According to various estimates, during the heating period, these premises' heat-generating devices consume from 40 to 90% of the total cost of fuel and power resources [5]. Hence, even partial reduction of these expenses will lead to a significant reduction in the livestock products' cost.

An effective way to reduce power consumption in livestock premises is to utilize ventilation emissions' heat to warm up supplied ventilation air. The difficulty of utilizing the ventilation emissions' heat lies in exhaust air's being a low-potential source of thermal energy [6].

To ensure air removal from piggery premises, an automatic ventilation system for polluted air intake from livestock premises was created [6]. As a result of analytical studies of this system, the conditions for its effective operation have been mathematically presented.

In the larger part of Ukraine, soil is the most accessible source of low-potential heat. At the depths of over 10 meters, it maintains constant its temperature ranging from +9 to 12°C throughout the year. This creates favorable conditions for an efficient use of heat pumps. Ukraine has a significant potential for using the heat of soil and groundwater [7]. The temperature of soil and rocks on the top of the ground depends on the balance of thermal energy coming from the Sun and thermal radiation from the earth surface. Thermal energy coming from the Sun gets accumulated in the layer of sedimentary strata and rocks at the depths up to the isothermal surface. This soil layer may be considered as a natural seasonal accumulator of thermal energy, since the energy withdrawn in winter period is restored in summer. This also applies to groundwaters, which saturate the upper layer of soil and sedimentary strata [8].

Analysis of technical means of thermal energy extraction from surface layers of soil [9–11] made it possible to determine that vertical-type ground heat exchangers are the most effective ones among considered options used to achieve required microclimate parameters in livestock premises. However, their optimal parameters, location and energy efficiency limits have not been sufficiently covered in the literature.

Relying on the analysis of previous studies of structural and process diagram of ground-based air heat exchanger, let us consider the two options being most cost-effective in terms of their manufacture. The first option is based on studies [12–14] – a concentric-type vertical ground heat exchanger. For this purpose, the structural and process parameters were chosen that were obtained as a result of experimental research (Fig. 1, a). The second option is a more classical one – the U-shaped vertical-type ground heat exchanger [15–16] (Fig. 1, b)

According to research [17] (in which water was the heat transfer agent), a concentric-type heat exchanger is the most effective one for short-term operation, but for long-term operation, its efficiency drops by 18–20%. In addition, our own experience in research of concentric-type heat exchangers [18] shows that a concentric-type pipe-in-pipe arrangement causes secondary temperature change through internal walls. This negatively affects the process of air flow heating or cooling the within soil. It should be noted that under internal walls' thermal insulation, sufficiently large non-operating zone is generated, this only leading to pneumatic losses.

Analytical studies of ground heat exchanger's pneumatic losses

The first stage in determining the most rational arrangement of ground-based air heat exchanger is calculation of air pumping power.

Let's divide the air path into five sections (Fig. 1). According to [19], pressure losses in each section are summarized in table. 1.

Table 1 – Pneumatic pressure losses in all sections of vertical-type ground heat exchangers

Area	Concentric-type	U-shaped
I	(1) $\Delta p_{CI} = 0{,}11\frac{273\rho_{н.у.}}{2TD_{CI}}L_C\left(\frac{4q_{in}}{\pi D_{CI}^2}\right)^2\left(\sqrt[4]{\frac{17\mu T\pi D_{CI}}{273q_{in}\rho_{н.у.}}}+\frac{\psi}{D_{CI}}\right)$	(6) $\Delta p_{UI} = 0{,}11\frac{273\rho_{н.у.}}{2TD_{UI}}L_U\left(\frac{4q_{in}}{\pi D_{UI}^2}\right)^2\left(\sqrt[4]{\frac{17\mu T\pi D_{UI}}{273q_{in}\rho_{н.у.}}}+\frac{\psi}{D_{UI}}\right)$
II	(2) $\Delta p_{CII} = \zeta_{CII}\frac{273\rho_{н.у.}}{2T}\left(\frac{4q_{in}}{\pi D_{CI}^2}\right)^2$	(7) $\Delta p_{UII} = 2\frac{273\alpha\rho_{н.у.}}{T}\left(\frac{4q_{in}}{\pi D_{UI}^2}\right)^2$
III	(3) $\Delta p_{CIII} = 0{,}11\frac{273\rho_{н.у.}(L_C-L_{CI})}{2T\sqrt{D_{C2}^2-D_{CI}^2}}\left(\frac{4q_{in}}{\pi D_{CI}^2}\right)^2\times\left(\sqrt[4]{\frac{17\mu T\pi D_{CI}^2}{273q_{in}\sqrt{D_{C2}^2-D_{CI}^2}\rho_{н.у.}}}+\frac{\psi}{\sqrt{D_{C2}^2-D_{CI}^2}}\right)$	(8) $\Delta p_{UIII} = 0{,}11\frac{273\rho_{н.у.}(L_U-L_{UI})}{2TD_{UI}}\times\left(\frac{4q_{in}}{\pi D_{UI}^2}\right)^2\left(\sqrt[4]{\frac{17\mu T\pi D_{UI}}{273q_{in}\rho_{н.у.}}}+\frac{\psi}{D_{UI}}\right)$
IV	(4) $\Delta p_{CIV} = \frac{273\alpha\rho_{н.у.}}{T}\left(\frac{4q_{in}}{\pi D_{CI}^2}\right)^2$	(9) $\Delta p_{UIV} = \frac{273\alpha\rho_{н.у.}}{T}\left(\frac{4q_{in}}{\pi D_{UI}^2}\right)^2$
V	(5) $\Delta p_{CV} = 0{,}11\frac{273\rho_{н.у.}}{2TD_{CI}}L_{C2}\left(\frac{4q_{in}}{\pi D_{CI}^2}\right)^2\left(\sqrt[4]{\frac{17\pi D_{CI}\mu T}{273q_{in}\rho_{н.у.}}}+\frac{\psi}{D_{CI}}\right)$	(10) $\Delta p_{UV} = 0{,}11\frac{273\rho_{н.у.}}{2TD_{UI}}L_{U2}\left(\frac{4q_{in}}{\pi D_{UI}^2}\right)^2\left(\sqrt[4]{\frac{17\pi D_{UI}\mu T}{273q_{in}\rho_{н.у.}}}+\frac{\psi}{D_{UI}}\right)$

where $\rho_{н.у.}$ = 1.293 kg/m^3 – air density under normal conditions; L – air duct length, m; T – air flow temperature, K; D – air duct diameter, m; q_{in} – input air flow rate, m^3/s; μ = 18.27·10^{-6} N·s/m^2 – dynamic air viscosity; ψ = 0.1 mm (for polyethylene) – equivalent roughness of air duct walls; ζ= 2 – local resistance coefficient for spatial (circular) rotation by 180° during injection; α= 0.55 – impact mitigation factor for a constant cross-section knee.

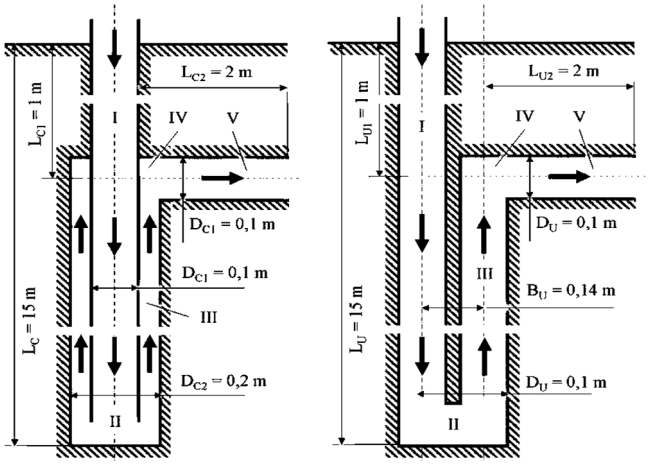

Fig. 1. Calculation model of vertical-type ground heat exchangers, a – concentric-type; b – U-shaped

Pressure losses in the heat exchanger can be calculated as the sum of all pressure losses in each section

(11) $$\Delta p_{ST} = \Delta p_I + \Delta p_{II} + \Delta p_{III} + \Delta p_{IV} + \Delta p_V.$$

Also, the power required for air pumping through a vertical heat exchanger is determined using the formula:

(12) $$N_{ST} = \frac{q_{in}\,\Delta p_{ST}}{\eta_п}$$

where $\eta_п$ is the fan's overall efficiency, $\eta_п$ = 0.85.

Having performed a joint calculation of dependencies (1)–(12) using Wolfram Cloud software, we obtained the dependencies between pneumatic losses' power change N_{ST} of U-shaped vertical-type ground heat exchanger and its length L_{U1}, diameter D_{U1} and air flow injection q_{in} shown in Fig. 2.

Comparing the power values of pneumatic losses in concentric-type and U-shaped heat exchangers, it was determined that the power of the latter is higher by 0.9–1.7%. That is, air losses in both options of vertical-type ground heat exchangers are almost the same. Therefore, to evaluate the efficiency, one should investigate their heat capacity.

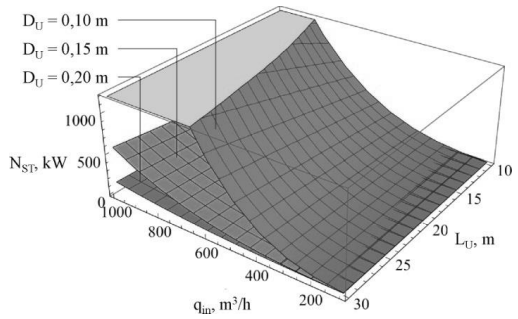

Fig. 2. Dependencies between pneumatic losses' power change N_{ST} of U-shaped vertical-type ground heat exchanger and its length L_{U1} , diameter D_{U1} and air flow injection q_{in}

Physical-and-mathematical apparatus of air flow heating process in a vertical-type ground heat exchanger

The second stage involves the physical-and-mathematical apparatus of air flow heating process in a vertical-type ground heat exchanger.

Calculation models of two options of vertical-type ground heat exchangers housed in the ventilation system for clean air injection [20–21] are shown in fig. 3.

A rectangular coordinate system is chosen in such a way that axis OX is directed along the horizon and parallel to the axis of the heat exchanger's horizontal section, with axis OY being directed perpendicular to the plane of the figure, and OZ axis directed vertically down.

We take the following assumptions [22]:

– the soil is homogeneous and isotropic, and its thermophysical properties remain unchanged when temperature changes;

– the thermal contact between the ventilation system's wall and surrounding soil is ideal;

- due to a slight change in the air flow pressure during its movement in the ventilation system, air is deemed to be an incompressible liquid.

The heat flowing through the ventilation system's surface S at a given moment of time τ can be represented by formula [23-24]

$$\frac{dq}{d\tau} = -\lambda_S \int_S \frac{\partial T_S}{\partial n} dS \tag{13}$$

where T_S (x,y,z,τ) is the temperature at the soil point, which has coordinates (x, y, z) at time moment τ, °C .

The continuity equation that reflects the fact that there are no voids and gaps in the field occupied by air M_{air}, in the accepted rectangular coordinate system, has the following form

$$\frac{\partial u}{\partial x} + \frac{\partial v}{\partial y} + \frac{\partial w}{\partial z} = 0, \ (x,y,z) \in M_{air} \tag{14}$$

where u, v, w are velocity components in x, y, z directions.

Air movement in such a case is described by Navier-Stokes equations, which take the form for a rectangular coordinate

$$\begin{aligned} \rho\frac{Du}{\partial\tau} &= \frac{\partial p}{\partial x} + \mu\nabla^2 u, \qquad \rho\frac{Dv}{\partial\tau} = \frac{\partial p}{\partial y} + \mu\nabla^2 v, \\ \rho\frac{Dw}{\partial\tau} &= \frac{\partial p}{\partial y} + \mu\nabla^2 w, \qquad (x,y,z) \in M_{air}. \end{aligned} \tag{15}$$

Substantial derivatives making part of the previous equations are expressed by the following dependencies:

$$\begin{aligned} \frac{Du}{\partial\tau} &= \frac{\partial u}{\partial\tau} + u\frac{\partial u}{\partial x} + v\frac{\partial u}{\partial y} + w\frac{\partial u}{\partial z}, \\ \frac{Dv}{\partial\tau} &= \frac{\partial v}{\partial\tau} + u\frac{\partial v}{\partial x} + v\frac{\partial v}{\partial y} + w\frac{\partial v}{\partial z}, \\ \frac{Dw}{\partial\tau} &= \frac{\partial w}{\partial\tau} + u\frac{\partial w}{\partial x} + v\frac{\partial w}{\partial y} + w\frac{\partial w}{\partial z}. \end{aligned} \tag{16}$$

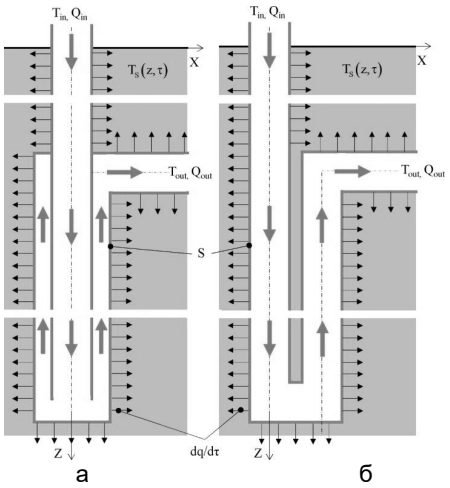

Fig. 3. Calculation models of concentric-type (a) and U-shaped (b) vertical-type ground heat exchangers of the clean air injection system

The Laplace operator in a rectangular coordinate system has the following form^

$$\nabla^2 = \left(\frac{\partial^2}{\partial x^2} + \frac{\partial^2}{\partial y^2} + \frac{\partial^2}{\partial z^2} \right). \tag{17}$$

The temperature field in a moving air flow is described by energy equation [25–26]

$$\frac{DT_a}{\partial\tau} = a_a \nabla^2 T_a, \quad (x,y,z) \in M_a, \tag{18}$$

where T_a (x,y,z,τ) is the air temperature at the air point, which has coordinates (x,y,z) at time moment τ, °C.

The derivative included in previous equation (18) is written as follows

$$\frac{DT_a}{\partial\tau} = \frac{\partial T_a}{\partial\tau} + u\frac{\partial T_a}{\partial x} + v\frac{\partial T_a}{\partial y} + w\frac{\partial T_a}{\partial z}. \tag{19}$$

The temperature field in the soil stratum is described by the following thermal conductivity equation [27–28]

$$\frac{\partial T_s}{\partial\tau} = a_s \nabla^2 T_s, \quad (x,y,z) \in M_s, \tag{20}$$

Initial conditions [29]

$$\begin{cases} T_S(x,y,z,0) = T_{S0}(z), & (x,y,z) \in M_S, \\ T_a(x,y,z,0) = T_{a0}(z), & (x,y,z) \in M_a. \end{cases} \tag{21}$$

Boundary conditions

$$\begin{cases} T_a(x,y,0,\tau) = T_l(x,y), & (x,y,z) \in M_a, \\ T_S(x,y,0,\tau) = f(\tau), & (x,y,z) \in M_a. \end{cases} \tag{22}$$

where T_S (x,y,0,τ) is the function that determines the soil surface temperature and depends on natural and climatic conditions [30–33]:

$$T_S(z,\tau) = T_m - A_s e^{-z\sqrt{\frac{\pi}{365\alpha_s}}} \cos\left(\frac{2\pi}{365}\left(\tau - \tau_0 - \frac{z}{2}\sqrt{\frac{365}{\alpha_s \pi}} \right) \right) \tag{23}$$

where T_S (z, τ) is the soil temperature at time τ and depth z, °C; T_m – the average soil surface temperature, °C; A_s – the amplitude of soil surface change, °C; α_s – thermal

conductivity coefficient of the soil, m^2 /day; τ – the time elapsed since the beginning of the calendar year, day; τ_0 is the phase constant of the soil surface, day.

The condition of heat flow density equality on the ground heat exchanger's wall

$$\alpha = -\frac{\lambda_a}{T_a - T_s}\frac{\partial T_a}{\partial n}. \quad (24)$$

By approximating the ten-year data on the temperature on the surface of Vinnytsia region soils [34] in the form of a cosine function, we got the graph shown in Fig. 4.

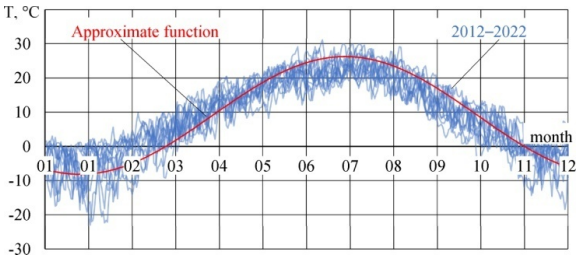

Fig. 4. Soil surface temperature according to long-term observations in Vinnytsia region

Taking into account the approximated data, the values of T_m = 9.79°C, A_s = 22.005°C, τ_0 = 23 days were determined. The coefficient of soil thermal conductivity α_s = 0.0253-0.089 m^2 /day depends on soil density, humidity and type. For further calculations we assume the largest value of soil thermal conductivity coefficient α_s = 0.089 m^2 /day. Then, by substituting the obtained values into equation (23), we obtain graphs of soil temperature distribution by depth (Fig. 5)

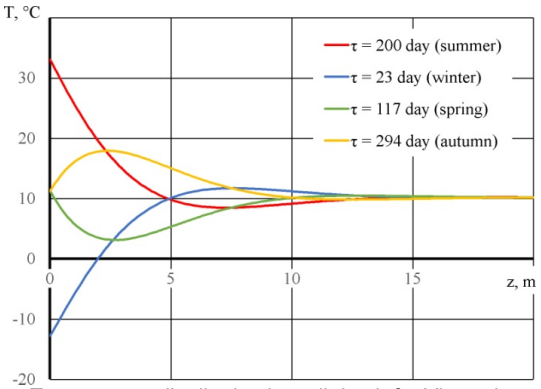

Fig. 5. Temperature distribution by soil depth for Vinnytsia region

It was determined from Figure 5 that for natural and climatic conditions of Vinnytsia region, soil temperature fluctuations are the smallest ones (0.5°C) starting from depth z = 12.3 m, which can be taken as the smallest effective depth for the ground heat exchanger.

The obtained results will be used for numerical modeling of vertical-type ground heat exchangers.

Results of numerical modeling of air flow heating process in vertical-type ground heat exchangers

At the third stage, provision is made for a numerical modeling of the air flow heating process in vertical-type ground heat exchangers.

Numerical modeling was performed using Simcenter Star-CCM+ software package, which employs the spatial discretization method to use the finite volume method with calculation of unknown cells in the centers. In order to reduce the number of finite elements' grid elements and to save computing resources, the symmetry area along plane XOZ was used.

The general appearance of the calculated grid, as well as structural-and-technological parameters of two options of vertical-type ground heat exchangers are shown in fig. 6.

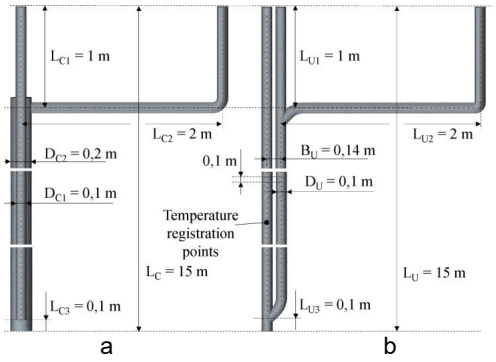

Fig. 6. General view of the calculated grid, as well as structural-and-technological parameters of concentric-type (a) and U-shaped (b) vertical-type ground heat exchangers

The following were selected as physical models of air: the three-dimensional one, the Eulerian multiphase model, VOF method of separated flow and volume liquid, the phase interaction model and the model of separated multiphase temperature. Current flow is subject to the Navier-Stokes equation and k-ε model of turbulence. Euler phases were air and water. The air phase was subjected to MASVP-PR97 real gas (vapor) and turbulent flow models. The water phase obeyed the van der Waals real gas and turbulent flow models [35]

Physical models of the walls of the ventilation system for clean air injection are as follows: three-dimensional model of solid body material, constant density and the model of separated solid body's energy.

The following models were selected as physical models of soil: three-dimensional model of solid body material, constant density and the model of separated solid body's energy.

Temperature distribution in soil is subject to equation (23), i.e. fig. 5.

A non-stationary implicit solver was chosen. The number of internal inertias was equal to 10. Total simulation time – 10^5 s.

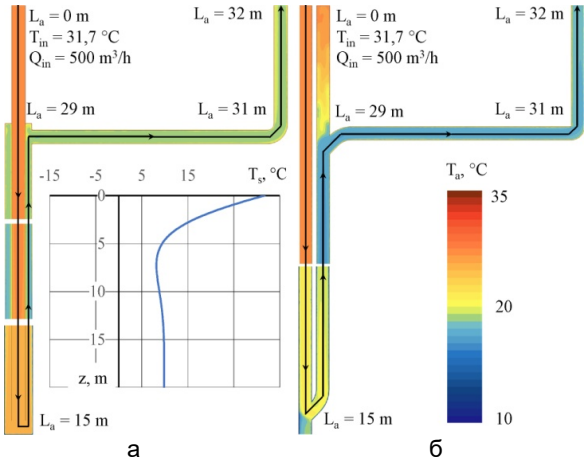

Fig. 7. Temperature field distribution in concentric-type (a) and U-shaped (b) vertical-type ground heat exchangers in summer period with the air injection of 500 m^3 /h

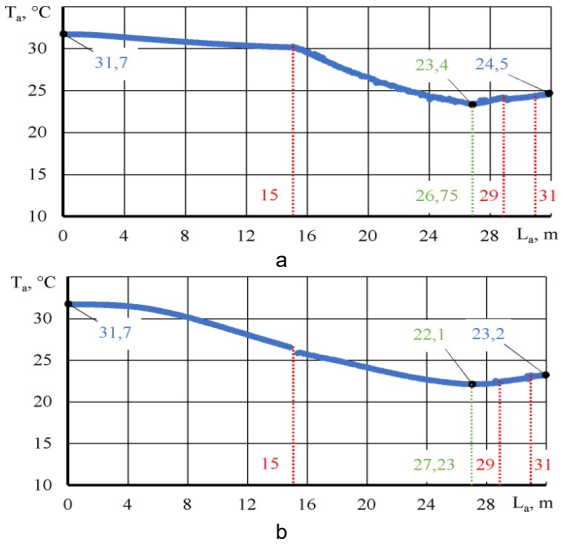

Fig. 8. Graph of dependence between air flow temperature T_a and its path L_a in concentric-type (a) and U-shaped (b) vertical-type ground heat exchangers in summer period with the air injection of 500 m^3/h

According to the simulation results, the distribution of the temperature field in vertical-type ground heat exchangers in summer period was obtained (Fig. 7).

For more accurate display of simulation results, the graph of dependence between air flow temperature T_a and its path L_a was plotted , which is shown in Fig. 8.

It follows from fig. 7–8 that summer temperature of the air flow, which moves along the pipes with the total length of 32 m, decreases from 31.7°C to 24.5°C in concentric-type heat exchangers and to 23.2°C in U-shaped heat exchangers.

That is, the largest temperature difference is observed for the U-shaped heat exchanger (8.5°C) as opposed tot the value of the concentric-type heat exchanger (7.2°C).

By analyzing the graphs in fig. 8, it was determined that the lowest temperature observed for the air flow path is 26.75 m (concentric-type heat exchanger) and 27.23 m (U-shaped heat exchanger), being 23.4°C and 22.1°C, respectively. This testifies to the need for the air duct's thermal insulation at the depth of approximately 2.77–3.25 m, this to ensure preservation of the lowest temperature right up to the exit from the heat exchanger.

Let us conduct a similar analysis with respect to the results of the numerical simulation in winter period. Temperature distributions and graphs of temperature changes are shown in fig. 9–10.

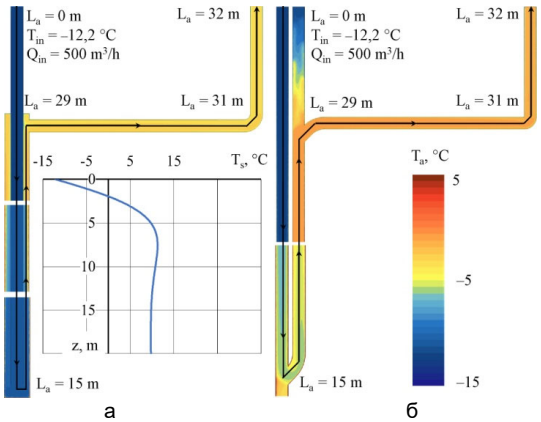

Fig. 9. Temperature field distribution in concentric-type (a) and U-shaped (b) vertical-type ground heat exchangers in winter time period with the air injection of 500 m^3/h

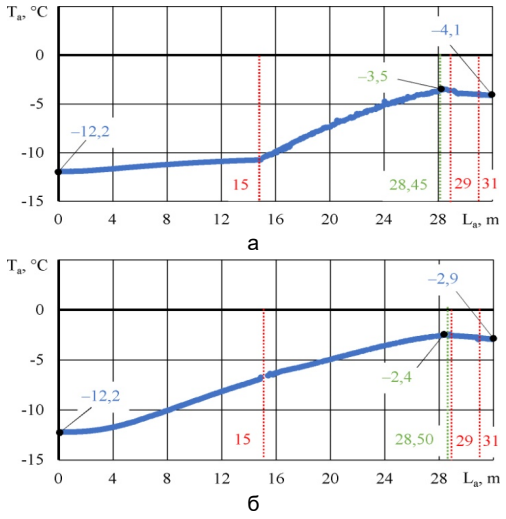

Fig. 10. Graph of dependence between air flow temperature T_a and the path of its movement L_a for concentric-type (a) and U-shaped (b) vertical-type ground heat exchangers in winter period with the air injection of 500 m^3/h

It was determined from fig. 9–10 that winter-period temperature of the air flow that moves along pipes with the total length of 32 m, increases from –12.2 °C to –4.1 °C for the concentric-type heat exchanger and to –2.9 °C for U-shaped heat exchanger. That is, the largest temperature difference is observed for the U-shaped heat exchanger (9.3 °C) as opposed tot the value of the concentric-type heat exchanger (8.1 °C).

Analyzing the graphs shown in fig. 10, it was determined that the highest temperature is observed for the air flow path of 28.45 m (concentric-type heat exchanger) and 28.50 m (U-shaped heat exchanger), being –3.5°C and –2.4°C, respectively. This confirms the previous conclusion regarding the need for the air duct's thermal insulation at the depth of 1.50–3.25 m.

In future, we are going to use air ducts' thermal insulation at the depth of 1.50–2.77 m and take into account the lowest temperature at the exit from the heat exchanger.

To substantiate rational mode parameters, we are going to vary them within the following limits:

– inlet air temperatures T_{in} : –12.2°C, –1.225°C, 9.75°C, 20.725°C and 31.7°C;

– air consumption Q_{in} : 200 m^3/h, 350 m^3/h, 500 m^3/h, 650 m^3/h and 800 m^3/h.

According to the results of numerical modeling using Simcenter Star-CCM+ software package, processing of the data obtained using Wolfram Cloud software package made it possible to obtain a second-order regression equation that shows the dependence between the change in air flow temperature ΔT_a and research factors in the following form for each option of heat exchangers (Fig. 11):

– concentric-type heat exchanger

(25) $$\Delta T_{aC} = 5{,}91513 - 0{,}00720618\, Q_{in} - 0{,}323773\, T_{in} + 0{,}0161927\, T_{in}^2;$$

– U-shaped heat exchanger

(26) $$\Delta T_{aU} = 7{,}81976 - 0{,}00955501\, Q_{in} - 0{,}42689\, T_{in} + 0{,}000105189\, Q_{in}\, T_{in} + 0{,}018366\, T_{in}^2.$$

Figure 11 shows the dependence between changes in air flow temperature ΔT_a and inlet air temperature T_{in}, as well as air consumption Q_{in} for concentric-type and U-shaped vertical-type ground heat exchangers. It has been clearly determined that the difference is greater for the U-shaped heat exchanger. The increase in air consumption Q_{in} also leads to decrease in ΔT_a. The highest value of ΔT_a was observed for high (summer period, 31.7°C) and low (winter period, –12.2°C) temperatures. For the temperature

of 9.6°C, the lowest value of ΔT_a was observed, which is quite logical, since soil temperature at the depth of over 12.3 m is T_m = 9.79°C.

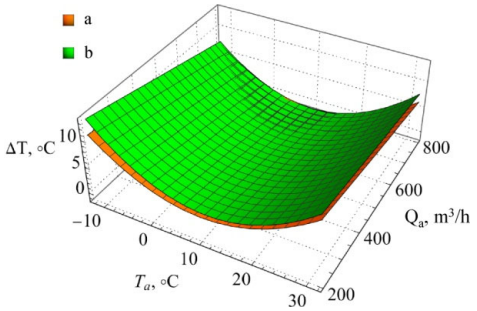

Fig. 11. Graphs of dependence between the change in air flow temperature ΔT_a and research factors for concentric-type (a) and U-shaped (b) vertical-type ground heat exchangers

Statistical analysis of equations (25) and (26) in studied variation range showed that Pearson correlation coefficient is 0.94. Fisher's test is also F = 2.12 < F_t = 2.49. This confirms the adequacy of the model obtained.

As mentioned before, during air flow's passage through the ground heat exchanger, it interacts with the air duct's walls, this causing pneumatic losses. Therefore, ground heat exchanger's effective heat capacity was chosen as the optimization criterion, which can be calculated as follows:

(27) $$N_E = N_T - N_{ST}$$

where N_T is the ground heat exchanger's heat capacity, W and N_{ST} is the power required to pump air through the ground heat exchanger, W.

The ground heat exchanger's heat capacity can be determined as follows:

(28) $$N_T = \frac{Q_{in}}{3600}\rho_a(T_{in})c_a\Delta T_a$$

where Q_{in} – the volumetric air injection, m³/h; $\rho_a(T_{in}) = \frac{273}{273+T_{in}}$ – air density at the heat exchanger's outlet, kg/m³; c_n – specific heat capacity of air assumed as c_n = 1003.62 J/(kg·°C); ΔT_a being the temperature difference at the heat exchanger's inlet and outlet, °C.

By combining the equations and using the Wolfram Cloud software package, we obtain the dependencies between the effective heat capacity of ground heat exchangers N_E and incoming air temperature T_i, as well as air consumption Q_{in}, as shown in Fig. 12.

Taking into account the condition of maximization of ground heat exchangers' effective heat capacity N_E, defined were rational air consumption values Q_{in} = 453.8 m³/hour concentric-type heat exchanger and Q_{in} = 455.2 m³/hour for U-shaped heat exchanger.

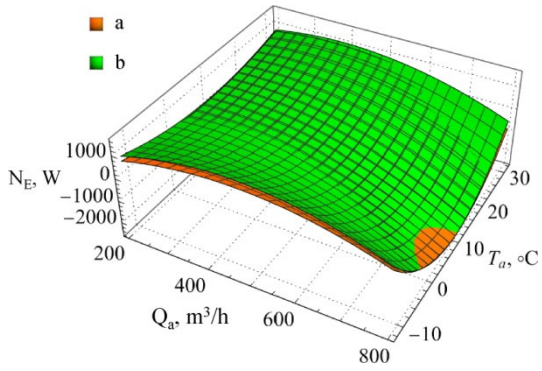

Fig. 12. Graphs of dependence between changes in ground heat exchangers' effective heat capacity N_E and research factors for concentric-type (a) and U-shaped (b) vertical-type ground heat exchangers

Thus, the effective heat capacity of concentric-type heat exchanger is N_{EC} (T_{in} = 31.7 °C) = 1266 W, N_{EU} (T_{in} = –12.2 °C) = 1052 W, which is less than effective heat capacity of U-shaped heat exchanger N_{EU} ($_{in}$ = 31.7°C) = 1575 W, N_{EU} (T_{in} = –12.2°C) = 1235 W. That is, U-shaped vertical-type ground heat exchangers are 17–24% more efficient than concentric-type ones.

Results of experimental studies of air flow heating process in vertical-type ground heat exchangers

At the fourth stage, provision is made for experimental studies of air flow heating process in vertical-type ground heat exchangers in production conditions at a pig farm of Agrofirma Napadivs'ka (Napadivka village, Vinnytsia district).

To raise the efficiency of clean air injection system's operation, a U-shaped vertical-type ground heat exchanger was installed behind the pig fattening premises. The ground heat exchanger's outlet pipe is connected to one of the clean air injection system's lines at the depth of 1 m from the soil surface. The well's total length is 18 m. At the depth of 3 m, the duct was thermally insulated. The last 3 m are made to collect condensed water. The structural-and-technological diagram and the general appearance of the experimental installation are shown in fig. 13.

Cimatic parameters of the research were determined based on the data of temperature and air humidity measurements at the beginning of each series of measurements and entered into Excel data table.

According to the results of numerical modeling of the air flow heating process in a vertical-type ground heat exchanger, it can be concluded that its nature depends on a number of factors. Accordingly, during experimental studies of this process, one should proceed from the technological possibilities of parameter change, and this requires conducting a large number of experiments. To reduce the number of experiments while preserving the reliability of technological process-related information, some methods of the experiment planning theory were used.

The process of heat extraction from the soil strata is influenced by: soil type and moisture, the operating time of geothermal ventilation system in a particular mode (supply air heating or cooling), ambient air temperature, volumetric air injection, diameter, length, number, interaxial distance and location of ground heat exchangers.

The soil type is low-humus black soil, on which the pig farm is located.

The dimensions were selected based on theoretical calculations.

DUNDAR CT 16.4 centrifugal fan was used as a power air plant (with the maximum air flow of 850 m³/h). The research was performed by varying the values of the following factors:

– the air flow at three levels: minimum (200 m³/h), average (500 m³/h) and maximum (800 m³/h), each of them to be determined after calibration by the electric fan motor's rotation speed and regulated by frequency converter FC 51 of VLT Micro series (current frequency 10; 30; 50 Hz) subject to a stable operation at specified frequency; air flow was measured using Solomat MPM 500E multifunctional device;

–air temperature in the ground heat exchanger was measured and recorded 6 times a day.

– Central air pumping duct air at the pig fattening farm was laid at the construction stage already, representing a tray of utility networks L 1-8/2 that passed under the pigs' room. Air injection nozzles that came out of the central air duct were polypropylene pipes.

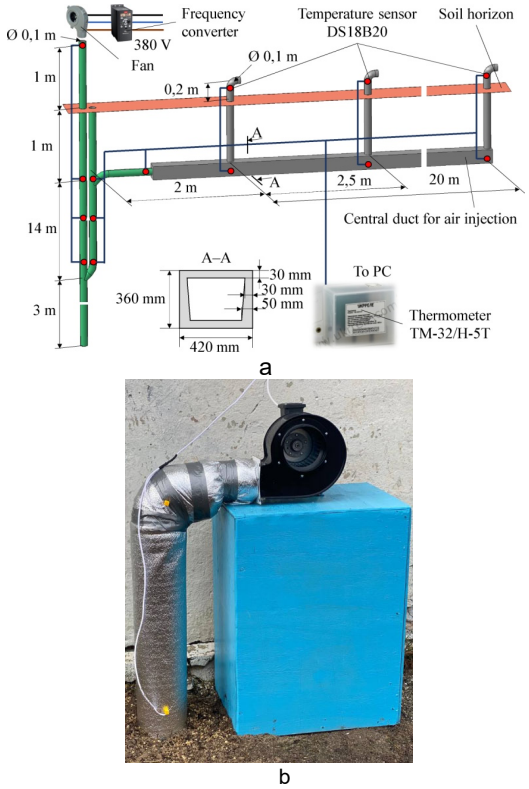

Fig. 13. Diagram (a) and general view (b) of the ground heat exchanger

DS18B20 digital temperature sensors are placed throughout the air injection system, which sensors are connected to «Termometr TM-32/N-5T» data recording system. The distance between the sensors in the ground heat exchanger was 3 m along the entire air duct.

The research was conducted in the period from 02.01.2021 to 02.01.2022.

During the research, the dynamics of temperature obtained from each sensor in the entire research period was recorded.

The centrifugal fan motor's power was determined by the frequency converter [36-37].

For typically low (in winter), high (in summer) and medium (in autumn and spring) temperatures T_{in}, air flow injection Q_{in} was varied.

The change in air flow temperature ΔT_a at the inlet and outlet of the ground heat exchanger was chosen as the research criterion. To optimize the parameters of the ground heat exchanger, heat capacity N_E criterion was used.

Figure 14 shows the dynamics of temperatures in the ground heat exchanger at different distances from duct L_a . The absolute value of the temperature difference at the ground heat exchanger's inlet and outlet Δ is also observed.

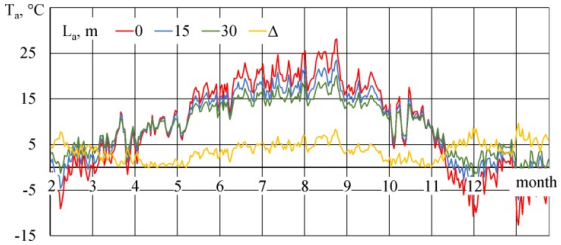

Fig. 14. Temperature dynamics in the ground heat exchanger at the duct's different distances

According to the research technique, air injection Q_{in} was varied at typically low (in winter), high (in summer) and medium (in autumn and spring) temperatures T_{in} . As such temperatures, the following ones were chosen: –12.2 °C, 9.8 °C and 28.1 °C. The graphs of temperature distribution in the heat exchanger's air duct for pumping Q_{in} = 500 m^3/h are shown in Fig. 15.

It can be seen from fig. 15 analysis that there is a temperature change trend along the entire air duct length, which trend is typical for numeric modeling results. That is why let us proceed to calculation of experimental regression equations and their comparison with theoretical ones.

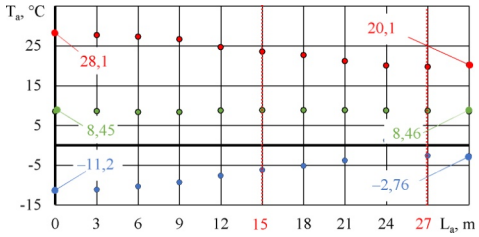

Fig. 15. Graph of experimental dependence between air flow temperature T_a and the path of its movement L_a in a U-shaped vertical-type ground heat exchanger with the air injection of 500 m^3/h

Upon their processing in Wolfram Cloud software package, the second-order regression equation was obtained, which shows the dependence between the change of air flow temperature ΔT_a in the U-shaped vertical-type ground heat exchanger and the research factors in the following form (Fig. 16):

(29) $\Delta T_{aU} = 8{,}77254 - 0{,}00956083\ Q_{in} - 0{,}322949\ T_{in} + 0{,}0000790378\ Q_{in}\ T_{in} + 0{,}0145349\ T_{in}^2$.

Visual analysis of fig. 16 testifies to the identity of theoretical and experimental dependencies. Pearson correlation coefficient equals to 0.94. Also, Fisher's criterion is $F = 2.02 < F_T = 2.49$. This confirms the adequacy of the model obtained. Therefore, theoretical dependencies can be used in further production calculations.

In connection with the similarity of theoretical and experimental regression equations of air flow temperature change ΔT_a in U-shaped vertical-type ground heat exchangers, let us conduct visual and statistical comparison of calculated thermal efficiency (Fig. 17).

Statistical comparison of experimental data with theoretical dependence according to Pearson's correlation coefficient – 0.95 and Fisher's test – $F = 1.93 < F_T = 2.98$ testifies to a high adequacy of theoretical dependence. Hence, in the future we are going to use obtained theoretical dependencies to calculate the effective heat capacity of the U-shaped vertical-type ground heat exchanger.

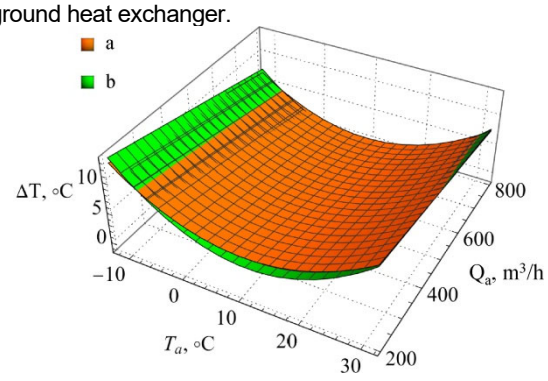

Fig. 16. Graphs of theoretical (a) and experimental (b) dependencies between air flow temperature change ΔT_a and research factors for U-shaped vertical-type ground heat exchangers

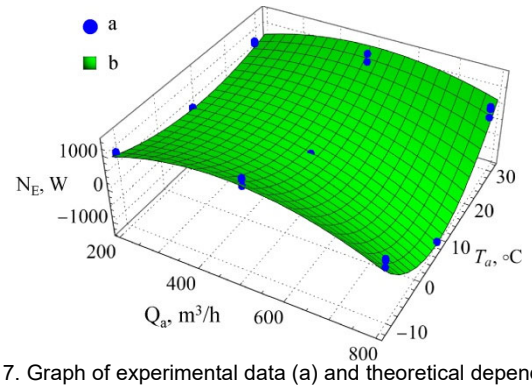

Fig. 17. Graph of experimental data (a) and theoretical dependence (b) between changes in the effective heat capacity of U-shaped vertical-type ground heat exchangers N_E and research factors

Conclusions

The results of analytical studies on the air losses of vertical ground heat exchangers for two proposed schemes (concentric and U-shaped) have determined that the power of the U-shaped heat exchanger is higher by 0.9–1.7%. Therefore, it can be assumed that the air losses of both variants of vertical ground heat exchangers are nearly identical. The dependence of the change in air loss power (NST) of the U-shaped vertical ground heat exchanger on its length (LU1), diameter (DU1), and air flow rate (qin) has been determined.

The physical-mathematical apparatus of the air heating process in a vertical ground heat exchanger has been generalized, based on equations of air flow continuity, Navier-Stokes equations, heat transfer equations, initial, and boundary conditions. An approximated function of ground temperature at time τ and depth z has been used as boundary conditions. Considering the approximated temperature data on the surface of the ground in the Vinnytsia region, the distribution of ground temperature with depth z has been determined.

Based on the results of numerical modeling of the air heating process in concentric and U-shaped vertical ground heat exchangers using the Simcenter Star-CCM+ software package, the distribution of the temperature field during the summer and winter periods was obtained. The temperature of the airflow during the summer (winter) period, which moves along a pipe with a total length of 32 m, decreases (increases) by 7.2°C (8.1°C) for the concentric heat exchanger and up to 8.5°C (9.3°C) for the U-shaped heat exchanger. The lowest (highest) temperature for the summer (winter) period is observed for the airflow path between 26.75–28.50 m. This indicates the necessity of thermal insulation for the duct at a depth of 1.50–3.25 m, ensuring the preservation of the lowest temperature until the exit from the heat exchanger.

Processing of the obtained data in the Simcenter Star-CCM+ software package and subsequent analysis in the Wolfram Cloud software package allowed obtaining second-order regression equations showing the dependencies of the change in airflow temperature ΔT_a and the effective thermal power N_E of ground heat exchangers on the temperature of incoming air T_{in} and airflow rates Q_{in} for each variant of the heat exchangers. Rational values of airflow rates were determined considering the condition of maximizing the effective thermal power of ground heat exchangers: Q_{in} = 453.8 m³/h for the concentric heat exchanger and Q_{in} = 455.2 m³/h for the U-shaped heat exchanger. Consequently, the effective thermal power of the concentric heat exchanger is $N_{EC}(T_{in} = 31.7°C)$ = 1266 W, $N_{EU}(T_{in} = –12.2°C)$ = 1052 W, which is lower than the effective thermal power of the U-shaped heat exchanger: $N_{EU}(T_{in} = 31.7°C)$ = 1575 W, $N_{EU}(T_{in} = –12.2°C)$ = 1235 W. Thus, the U-shaped vertical ground heat exchanger is 17–24% more efficient than the concentric one.

Experimental studies of the air heating process in the U-shaped vertical ground heat exchanger under industrial conditions determined the dynamics of temperature changes throughout the year. Regression equations of the second order describing the change in airflow temperature ΔT_a and effective thermal power N_E as functions of temperature T_{in} and airflow rates Q_{in} at the inlet of the U-shaped vertical ground heat exchanger were obtained. Statistical comparison of experimental data with theoretical dependencies, using the Pearson correlation coefficient of 0.95 and the Fisher criterion $F = 1.93 < F_T = 2.98$, indicates the high adequacy of the theoretical dependencies.

Funding

This research was supported and funded by the Ministry of Education and Science of Ukraine under grant № 0123U101794.

***Authors**: KALETNIK Hryhorii – Dr. Sc. in Economics, Professor, Academician NAAS of Ukraine, Head of the Department of Administrative Management and Alternative Fuel Resources, Vinnytsia National Agrarian University (21008, 3 Soniachna str., Vinnytsia, Ukraine); YAROPUD Vitalii – PhD in Engineering, Associate Professor, Dean of the Faculty of Engineering and Technology, Vinnytsia National Agrarian University (21008, 3 Soniachna str., Vinnytsia, Ukraine), e-mail: yaropud77@gmail.com;* LUTKOVSKA Svitlana – *Dr. Sc. in Economics, Professor, Vice-rector for scientific, pedagogical and educational work, Vinnytsia National Agrarian University* (21008, 3 Sonyachna str., Vinnytsia, Ukraine); *ALIIEV Elchyn - professor, doctor of technical sciences, senior researcher Dnipro State Agrarian and Economic University (49600, Serhii Efremov Str., 25, Dnipro, Ukraine).*

REFERENCES

[1] Kukharchuk V.V., Katsyv S.Sh., Hraniak V.F., Madyarov V.G., Kyivskyi V.V., Prychepa I.V., Kotyra A., Yeraliyeva B., Kozbakova A. (2020). Analysis of dependency current harmonics on load and filter parameters for asymmetrical network models. Przeglad Elektrotechniczny. Vol. 96, № 9. P. 103-107. DOI: 10.15199/48.2020.09.22

[2] Kaletnik G.M. (2019). Prospects for increasing the energy autonomy of agricultural enterprises in the framework of the energy strategy of Ukraine. Bulletin of Agrarian Science of the Black Sea Region. Vol. 4. P. 90-98. https://doi.org/10.31521/2313-092X/2019-4(104)-10.

[3] Kaletnik G.M., Lutkovska S.M. (2022). Ecological modernization and organic production in the system of environmental security: monograph. Vinn. nats. agrar. un-t. Vinnytsia: VNAU. 356 p.

[4] Paziuk V., Vyshnevskiy V., Tokarchuk O., Kupchuk I. (2021). Substantiation of the energy efficient schedules of drying grain seeds. Bulletin of the Transilvania University of Braşov. Series II: Forestry, Wood Industry, Agricultural Food Engineering. Vol. 14 (63), № 2. P. 137-146. DOI: 10.31926/but.fwiafe.2021.14.63.2.13

[5] Yaropud V. (2021). Analytical study of the automatic ventilation system for the intake of polluted air from the pigsty. Scientific Horizons. Vol. 24. № 3. P. 19–27. DOI: 10.48077/scihor.24(3).2021.19-27

[6] Yaropud V., Hunko I., Aliiev E., Kupchuk I. (2021). Justification of the mechatronic system for pigsty microclimate maintenance. Agraarteadus. Vol. 32, № 2. P. 341–351. DOI: https://doi.org/10.15159/jas.21.23

[7] Dolgikh D.O. (2012). Analysis of operation and classification of soil heat exchangers. Collection of scientific works of the Institute of Mechanization of Animal Husbandry of the National Academy of Sciences «Mechanization, environmentalization and conversion of bio-raw materials in animal husbandry». Vol. 1(9). Zaporizhzhia. P. 56–63.

[8] Blázquez, C.S., Borge-Diez, D., Nieto, I.M., Martín, A.F., González-Aguilera, D. (2023). Multiparametric Evaluation of Electrical, Biogas and Natural Gas Geothermal Source Heat Pumps. In: Borge-Diez, D., Rosales-Asensio, E. (eds)

Geothermal Heat Pump Systems. Green Energy and Technology. Springer, Cham. https://doi.org/10.1007/978-3-031-24524-4_4
[9] Shakil Masum, Liangliang Jiang. (2023). Technical Performance Comparison of Horizontal and Vertical Ground-Source Heat Pump Systems. Journal of GeoEnergy. Article ID 6106360. https://doi.org/10.1155/2023/6106360
[10] Hałaj E, Pająk L, Papiernik B. (2020). Finite element modeling of geothermal source of heat pump in long-term operation. Energies. 13(6):1341. https://doi.org/10.3390/en1306134.
[11] Yaropud V., Kupchuk I., Burlaka S., Poberezhets J., Babyn I. (2022). Experimental studies of design-and-technological parameters of heat exchanger. Przeglad Elektrotechniczny. Vol. 98, № 10. P. 57–60. DOI: https://doi.org/10.15199/48.2022.10.10
[12] Kovyazin O.S., Dolgikh D.O. (2013). Ground heat exchanger construction justification. Bulletin of KhNUTSG named after P. Vasylenko. № 132. P. 167.
[13] Kovyazin O.S. (2018). Justification of the diameter of the casing pipe of the soil heat exchanger and air supply to it. Bulletin of the National Technical University «KhPI». Series: Energy and heat engineering processes and equipment, №. 12(1288). doi: 10.20998/2078-774X.2018.12.13
[14] Hrushetsky S.M., Yaropud V.M., Duganets V.I., Duganets V.I., Pryshliak V.M., Kurylo V.L. (2019). Research of constructive and regulatory parameters of the assembly working parts for potato harvesting machines. INMATEH - Agricultural Engineering. Vol. 59, № 3. P. 101–110. DOI: https://doi.org/10.35633/inmateh-59-11
[15] Zhengxuan Liu, Mingjing Xie, Yuekuan Zhou, Yingdong He, Lei Zhang, Guoqiang Zhang, Dachuan Chen (2023). A state-of-the-art review on shallow geothermal ventilation systems with thermal performance enhancement system classifications, advanced technologies and applications. Energy and Built Environment, Vol. 4, Issue 2. P. 148-168, https://doi.org/10.1016/j.enbenv.2021.10.003
[16] Kupchuk I., Voznyak O., Burlaka S., Polievoda Y., Vovk V., Telekalo N., Hontaruk Y. (2023). Information transfer with adaptation to the parameters of the communication channel. Przegląd Elektrotechniczny. Vol. 99, № 3. P. 194-199. DOI: 10.15199/48.2023.03.34
[17] Jalaluddin, Jalaluddin; Miyara, Akio; Tsubaki, Koutaro; and Yoshida, Kentaro. (2010). Thermal Performances Of Three Types Of Ground Heat Exchangers In Short-Time Period Of Operation. International Refrigeration and Air Conditioning Conference. Paper 1123. http://docs.lib.purdue.edu/iracc/1123
[18] Aliev E.B., Yaropud V.M. (2015). Comparative analysis of the results of theoretical and experimental studies of the process of functioning of the heat-utilizer for livestock premises. Design, production and operation of agricultural machines, Vol. 45, Part II. Kirovohrad: KNTU. P. 120-124.
[19] Zhukovsky S.S., Labai V.Y. (2003).Aerodynamics of ventilation. Lviv «Lviv Polytechnic». 370 p.
[20] Soni S.K., Pandey M., Bartaria V.N. (2015). Ground Coupled Heat Exchangers: A Review and Applications. Renewable and Sustainable Energy Reviews, Vol. 47, P. 83–92. https://doi.org/10.1016/j.rser.2015.03.014
[21] Spirin A., Kupchuk I., Tverdokhlib I., Polievoda Yu., Kovalova K., Dmytrenko V. (2022). Substantiation of modes of drying alfalfa pulp by active ventilation in a laboratory electric dryer. Przegląd Elektrotechniczny. Vol. 98, № 5. P. 11-15. DOI: 10.15199/48.2022.05.02
[22] Koviazin A.S., Velichko I.G. (2013). Influence of the material and casing wall thickness of a ground heat exchanger on energy extraction rate. Herald of national University «Lviv Polytechnic» «Power system. Engineering the environment. Automation», Vol. 758, pp. 57–62
[23] Benli H. (2013). A Performance comparison between a Horizontal Source and Vertical Source Heat Pump System for a Greenhouse heating in the Mild Climate Elazig, Turkey. Applied Thermal Engineering, 1(50), 197–206. https://doi.org/10.1016/j.applthermaleng.2012.06.005.
[24] Vedmitskyi Y.G., Kukharchuk V.V., Hraniak V.F., Vishtak I.V., Kacejko P., Abenov A. (2018) Newton binomial in the generalized Cauchy problem as exemplified by electrical systems. Proceedings of SPIE 10808, Photonics Applications in Astronomy, Communications, Industry, and High-Energy Physics Experiments, 2018, 7 p. DOI: 10.1117/12.2501600.
[25] Koviazin A.S. (2017). The rationale for the thickness of the thermal insulation the inner tube of ground heat exchanger. Herald of aeroenginebuilding, Vol. 1, P. 19–24.
[26] Paziuk V., Snezhkin Y., Dmytrenko N., Ivanov S., Tokarchuk O., Kupchuk I. (2022).Thermal and physical properties and heat-mass transfer processes of drying pumpkin seeds. Przegląd Elektrotechniczny. Vol. 98, № 7. P. 154-157. DOI: 10.15199/48.2022.07.25.
[27] Atam E., Helsen L. (2016). Ground-coupled Heat Pumps: Part 1 – Literature Review and Research Challenges in modeling and Optimal Control. Renewable and Sustainable Energy Reviews, Vol. 54, P. 1653–1667. https://doi.org/10.1016/j.rser.2015.10.007
[28] Chiasson A.D. (2010). Modeling horizontal ground heat exchangers in geothermal heat pump systems. Proceedings of the 2010 COMSOL Multiphysics Conference, Boston, Massachusetts
[29] Sivasakthivel T., Murugesan K., Sahoo P.K. (2014). Optimization of Ground Heat Exchanger Parameters of Ground Source Heat Pump System for Space Heating Applications. Energy, Vol. 78, P. 573–586
[30] Shevchenko I., Kovyazin A., Kamiński J.R., Szeptycki A. (2017). Simulation of thermal field in soil. Problemy Inżynierii Rolniczej, Vol. 1(95). P. 57–65.
[31] Ji Y., Qian H., Zheng X. (2017). Development and Validation of a Three-dimensional Numerical Model for predicting the Ground Temperature Distribution, Energy and Buildings, Vol. 140, P. 261–267. https://doi.org/10.1016/j.enbuild.2017.01.079
[32] Tsurkan O., Kupchuk I., Polievoda Y., Wozniak O., Hontaruk Y., Prysiazhniuk Y. (2022). Digital processing of one-dimensional signals based on the median filtering algorithm. Przeglad Elektrotechniczny. Vol. 98, № 11. P. 51-56. DOI:10.15199/48.2022.11.08
[33] Kobets A.S., Naumenko M.M., Ponomarenko N.O., Kharytonov M.M., Velychko O.P., Yaropud V.M. (2017). Design substantiation of the three-tier centrifugal type mineral fertilizers spreader. INMATEH - Agricultural Engineering. Vol. 53, № 3. P. 13–20.
[34] https://power.larc.nasa.gov/data-access-viewer/
[35] Aliyev E.B. (2023). Numerical modeling of agro-industrial production processes: a textbook. Kyiv: Agrarian Science, 340 p. ISBN 978-966-540-584-9. DOI: 10.31073/978-966-540-584-9
[36] Hraniak V.F., Kukharchuk V.V., Bogachuk V.V., Vedmitskyi Y.G., Vishtak I.V., Popiel P., Yerkeldessova G. (2018) Phase noncontact method and procedure for measurement of axial displacement of electric machine's rotor. Proceedings of SPIE 10808, Photonics Applications in Astronomy, Communications, Industry, and High-Energy Physics Experiments, 2018, 7 p. DOI: 10.1117/12.2501611.
[37] Hraniak V.F., Kukharchuk V.V., Kucheruk V., Khassenov A.K. (2018). Using instantaneous cross-correlation coefficients of vibration signals for technical condition monitoring in rotating electric power machines. Bulletin of the Karaganda University. «Physics» series. Vol. 89, № 1. P. 72-80.